Structure evolution and τ_f influence mechanism of $Bi_{1-x}Ho_xVO_4$ microwave dielectric ceramics for LTCC applications

Huaicheng Xiang , Yuheng Zhang , Junqi Chen , Yang Zhou , Ying Tang , Jinwu Chen , Liang Fang

PII: S1005-0302(24)00275-5
DOI: https://doi.org/10.1016/j.jmst.2024.01.070
Reference: JMST 5551

To appear in: *Journal of Materials Science & Technology*

Received date: 2 January 2024
Revised date: 23 January 2024
Accepted date: 24 January 2024

Please cite this article as: Huaicheng Xiang , Yuheng Zhang , Junqi Chen , Yang Zhou , Ying Tang , Jinwu Chen , Liang Fang , Structure evolution and τ_f influence mechanism of $Bi_{1-x}Ho_xVO_4$ microwave dielectric ceramics for LTCC applications, *Journal of Materials Science & Technology* (2024), doi: https://doi.org/10.1016/j.jmst.2024.01.070

Highlights

- The main mechanisms affecting temperature stability of $Bi_{1-x}Ho_xVO_4$ were revealed through ion polarization theory and bond valence theory.
- The change in τ_{am} caused by the rattling effect of cations is the physical essence that affects τ_f, and the rattling effect can be used as an effective mechanism to regulate τ_f in low-ε_r materials.
- The best microwave dielectric properties with ε_r = 16.6, $Q \times f$ = 18,400 GHz, and τ_f = +3.29 ppm/°C were obtained in the $Bi_{0.2}Ho_{0.8}VO_4$ ceramic.
- $Bi_{1-x}Ho_xVO_4$ was compatible with Ag electrodes, indicating its potential application in LTCC technology.

Research Article

Structure evolution and τ_f influence mechanism of $Bi_{1-x}Ho_xVO_4$ microwave dielectric ceramics for LTCC applications

Huaicheng Xiang[a, b, *], Yuheng Zhang[a], Junqi Chen[c], Yang Zhou[a], Ying Tang[a, b], Jinwu Chen[c, *], Liang Fang[b, *]

[a] Key Laboratory of Low-Dimensional Structural Physics and Application, Education Department of Guangxi Zhuang Autonomous Region, College of Physics and Electronic Information Engineering, Guilin University of Technology, Guilin 541004, China

[b] Guangxi Universities Key Laboratory of Non-Ferrous Metal Oxide Electronic Functional Materials and Devices, Guangxi Key Laboratory of Optical and Electronic Materials and Devices, College of Materials Science and Engineering, Guilin University of Technology, Guilin 541004, China

[c] School of Mechanical Engineering, Guilin University of Aerospace Technology, Guilin 541004, China

*Corresponding authors.

E-mail addresses: xianghc@glut.edu.cn (H.C. Xiang); cnchenjw@guat.edu.cn (J.W. Chen); fanglianggl001@aliyun.com (L. Fang).

Abstract

$Bi_{1-x}Ho_xVO_4$ ($0.1 \leq x \leq 0.9$) ceramics were prepared via a solid-state reaction method, and all the ceramics could be well densified in the 920−980 °C range. The ceramics

with $0.1 \leq x < 0.4$ were composed of both monoclinic scheelite (M) and tetragonal zircon (T) phases, and a single M phase could be obtained in the range of $x \geq 0.4$. The measured ε_r decreased from 58.9 (x = 0.1) to 14.7 (x = 0.9), so do the calculated values ($\varepsilon_{r(C-M)}$ = 34.3−12.1), and the main reason for $\varepsilon_r > \varepsilon_{r(C-M)}$ was the rattling of Ho^{3+} in the dodecahedron. Two points with zero τ_f appeared in $Bi_{1-x}Ho_xVO_4$ ($0 \leq x \leq 1$) ceramics, and the best microwave dielectric properties with ε_r = 16.6, $Q \times f$ = 18,400 GHz (f = 10.69 GHz), and τ_f = +3.29 ppm/°C were obtained in the $Bi_{0.2}Ho_{0.8}VO_4$ ceramic. The change in temperature coefficient of ionic polarizability ($\tau_{\alpha m}$) caused by the rattling effect of cations is the physical essence that affects τ_f. Therefore, the rattling effect can be used as an effective mechanism to regulate τ_f in low-ε_r materials. Furthermore, there was no chemical reaction between $Bi_{1-x}Ho_xVO_4$ and Ag electrode, which indicates potential applications in low-temperature co-fired ceramic (LTCC) technology.

Keywords: $Bi_{1-x}Ho_xVO_4$; Near-zero τ_f; Bond valence; Rattling effect; LTCC

1. Introduction

With the rapid development of 5G and 6G mobile communications technology, microwave dielectric ceramics are already being used extensively for filters, oscillators, and substrates [1–3], and their requirements for extremely low relative permittivity (ε_r = 4–15) are particularly prominent. At the same time, low dielectric loss (high $Q \times f$) and near-zero temperature coefficient of resonant frequency (τ_f) are essential for device stability [4, 5].

$BiVO_4$ is known to belong to the $A^{3+}B^{5+}O_4$-type compound family; however, when heating above 528 K, monoclinic $BiVO_4$ (space group $I2/b$) undergoes a reversible ferroelastic phase transition to a tetragonal scheelite type structure (space group $I4_1/amd$) [6]. Meanwhile, the microwave dielectric properties of $BiVO_4$ ceramic were also reported, with an ε_r of 68, $Q \times f$ of 6,500 to 8,000 GHz, a large negative τ_f of −260 to −243 ppm/°C, and a sintering temperature below 900 °C [7, 8]. Nevertheless, the large negative τ_f value limited the practical application. Recently, it has been found that by replacing Bi with RE ions, τ_f can be increased by forming a series of tetragonal solid solutions. For example, $(1-x)BiVO_4$–$xYVO_4$ (ε_r = 45, $Q \times f$ = 14,000 GHz, and τ_f = +10 ppm/°C) [9] and $(Bi_{1-x}Ce_x)VO_4$ (ε_r = 11.9−47.9, $Q \times f$ = 18,000−22,360 GHz, and τ_f = +6.6− +15 ppm/°C) [10, 11] systems. It is worth noting that two-component points with near-zero τ_f appear in $(Bi_{1-x}Ce_x)VO_4$ (x = 0−1) ceramics, which are x = 0.25 and 0.95, respectively. However, the formation mechanism of near-zero τ_f has not been clarified.

The visual factors affecting τ_f mainly include the temperature coefficient of permittivity (τ_ε) and linear expansion coefficient (α_L) [$\tau_f = -(0.5\tau_\varepsilon + \alpha_L)$] [12]. Bosman and Havinga [13] pointed out the factors affecting τ_ε by differentiating the Clausius-Mosotti equation: (i) the volume expansion effect and (ii) the temperature dependence of polarizability. Harrop [14] assumed the temperature coefficient of polarizability ($\tau_{\alpha m}$) was negligible and discovered $\tau_f \propto \varepsilon_r$ in medium and high permittivity materials, that is, the “dilution of average ion polarizability” mechanism [15]. Recently, Fang’s team [16], in low-ε_r garnet ($A_3B_2C_3O_{12}$), found that small ions

entering the A-site caused a strong rattling effect, resulting in increased dielectric polarization, and τ_ε from positive to negative and τ_f from negative to positive. This was referred to as the "rattling" mechanism of regulating τ_f, and it has been further verified in garnet $Y_{3-x}R_xAl_{(Oct)2}Al_{(Tet)3-x}Si_xO_{12}$ (R = Mg, Ca) [17] and spinel $LiGa_5O_8$ [18] systems. These mechanisms provide valuable methods for the design of temperature-stable microwave dielectric ceramics. Considering the ionic radius of Ho^{3+} (1.015 Å, CN = 8) is smaller than that of Bi^{3+} (1.17 Å, CN = 8), the same is true for ionic polarizability, the rattling effect of dodecahedral cations is expected to be formed. Therefore, the $Bi_{1-x}Ho_xVO_4$ ($0.1 \le x \le 0.9$) ceramics were prepared using the solid-state reaction method. The structure evolution was investigated by X-ray diffractometer (XRD) refinement, and the regulation rule and mechanism of τ_f in microwave dielectric ceramics with low permittivity were discussed systematically by ion polarization and bond valence theory.

2. Methods

2.1. Sample Preparation

The $Bi_{1-x}Ho_xVO_4$ ($0.1 \le x \le 0.9$) ceramics, denoted as BHV-x, were synthesized through a conventional solid-state reaction method. The raw material Ho_2O_3 (99.99%, Aladdin) was dried at 900 °C for 1 h before being weighed. Ho_2O_3, Bi_2O_3 (99.99%, Aladdin), and NH_4VO_3 (99.95%, Aladdin) powders were ball-milled for 4 h and calcined at 860 °C for 4 h. The calcined powders were granulated with 5 wt.% poly(vinyl alcohol) (PVA), sieved using a 120 μm mesh, and then pressed into cylinders with a diameter of 10 mm and a thickness of 5 mm at a pressure of 200 MPa.

After burning off the PVA binder at 550 °C, these samples were sintered into dense bulks in the 920−980 °C range.

2.2. Characterization

The crystal structure and phase purity of the ceramics were studied by an XRD (Cu$K_{\alpha 1}$, 1.54059 Å, X'Pert PRO, PANalytical, Holland). The results were analyzed using the Rietveld profile refinement method with the FULLPROF program. The surface micrographs of the samples were observed via scanning electron microscopy (SEM, S4800, Hitachi, Japan). The Raman spectra at room temperature were obtained with a Raman spectrometer (DXR, Thermo Fisher Scientific, American) excited by an Ar^+ laser (780 nm). The bulk density of sintered pellets was determined by Archimedes method. The microwave dielectric properties were measured using a network analyzer (N5230A, Agilent) and a temperature chamber (Delta 9039, Delta Design). The τ_f and τ_ε at 25 °C (T_1) to 85 °C (T_2) were calculated as follows:

$$\tau_f = \frac{f_{T2} - f_{T1}}{f_{T1} \times (T_2 - T_1)} \quad (1)$$

$$\tau_\varepsilon = \frac{\varepsilon_{rT2} - \varepsilon_{rT1}}{\varepsilon_{rT1} \times (T_2 - T_1)} \quad (2)$$

3. Results and discussions

Fig. 1 shows the XRD patterns of the BHV-x ($0.1 \le x \le 0.9$) samples sintered at different temperatures. Both peaks of monoclinic scheelite (M PDF# 83-1699) and tetragonal zircon (T, PDF# 82-1973) phases can be observed within $0.1 \le x \le 0.2$. The large difference between the ionic radii of Bi^{3+} and Ho^{3+} (1.17 Å and 1.015 Å, respectively) determined that Ho^{3+} cannot enter the A-site of M but is rearranged with

the [VO_4] tetrahedra and formed the $HoVO_4$ with zircon structure. The intensity of the T phase increases continuously with the increase of Ho^{3+} content, whereas the intensity of the M phase decreases. For the BHV-0.4 sample, the prominent peaks of the M phase can hardly be observed. The content ratio of the T phase could be calculated approximately using the following equation [9]:

$$\text{Content of T phase} = \frac{I_T(200)}{I_T(200) + I_M(112)} \quad (3)$$

The ratio of the T phase increases with increasing x values, and the contents in 0.1, 0.15, and 0.2 are 25.92%, 50.06%, and 63.80%, respectively.

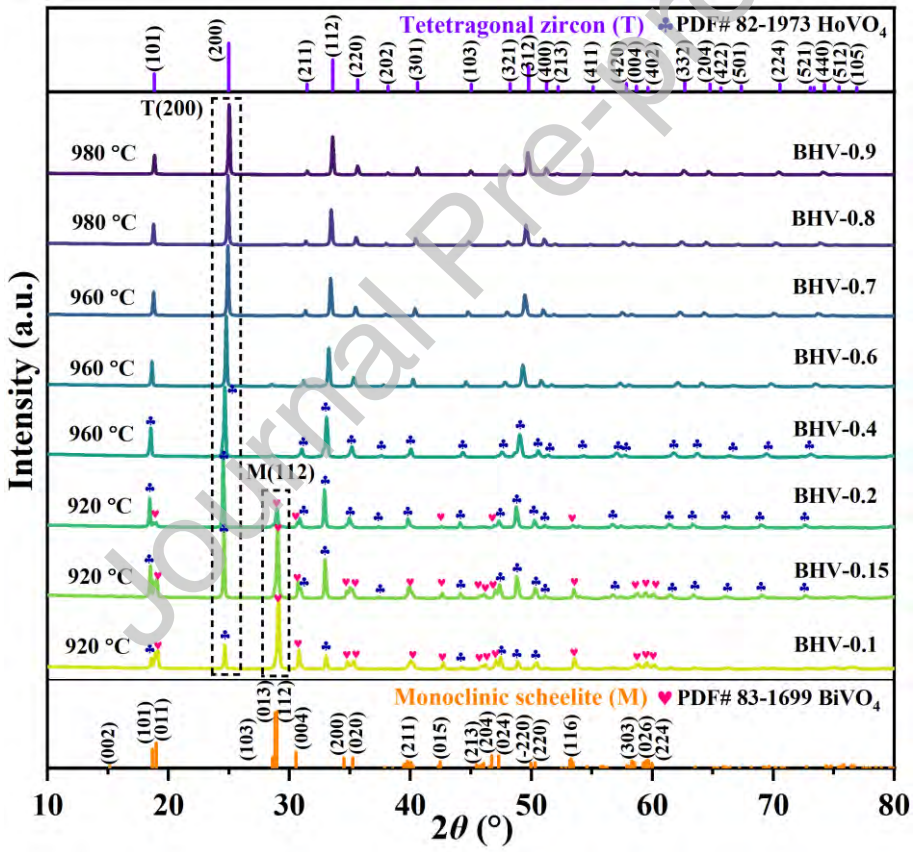

Fig. 1. XRD patterns of the $Bi_{1-x}Ho_xVO_4$ ($0.1 \leq x \leq 0.9$) ceramics sintered at optimal temperatures.

Rietveld structure refinement was performed on X-ray diffraction data of all samples

(Fig. S1 in Supplementary Information (SI)), and the observed and calculated XRD patterns of BHV-0.1, BHV-0.2, BHV-0.4, and BHV-0.8 samples are shown in Fig. 2(a−d). The refined lattice parameters for M and T phases ($BiVO_4$ and $Bi_yHo_{1-y}VO_4$ compositions were supposed) in the $x < 0.4$ samples. It reveals that the fractions of the M and T phases are about 67.8 wt.% and 32.2 wt.% for $x = 0.10$, 44.2 wt.% and 55.8 wt.% for $x = 0.15$, and 28.1 wt.% and 71.9 wt.% for $x = 0.20$, respectively. When $x \geq 0.4$, the patterns can be fitted excellently with a T structure (space group $I4_1/amd$). The refined profile agrees with the XRD pattern for each composition, and the reliability factors are reasonable (R_{wp} = 6.59%−8.84%, R_p = 4.68%−6.51%) (Fig. S1 and Table S1 in SI). Moreover, the lattice parameters (a, b, and c) unit cell volumes (V) of M and T phases both decrease with the increase of x (Fig. 3). In the $Bi_{1-x}Ho_xVO_4$ ($0.1 \leq x \leq 0.9$) ceramics, the Bi^{3+} (1.17 Å) at the A-site is substituted partially by the smaller-size Ho^{3+} (1.015 Å). The decrease of V is possibly associated with the contraction of parts of $[AO_8]$ dodecahedron. Fig. 2(e) shows the crystal structures of the M and T phases of AVO_4. In the M structure, the V^{5+} is coordinated tetrahedrally to oxygen with two different bond lengths, and the Bi^{3+} is coordinated to eight oxygens with four different bond lengths. The coordination environment in the $HoVO_4$ with zircon structure is the same as that in monoclinic $BiVO_4$. When cations with smaller radii replace Bi^{3+} at the A-site, the internal stress of the crystal increases, resulting in Bi−O fracture and then re-polymerization to form a transition of monoclinic phase and tetragonal phase [19, 20].

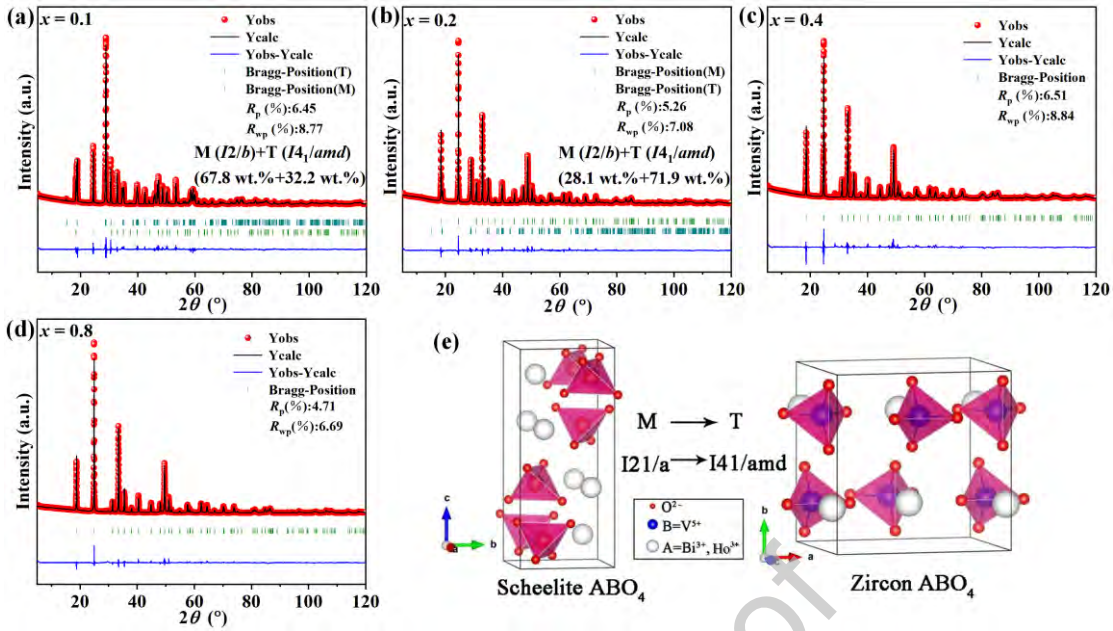

Fig. 2. Rietveld refinements for (a) x = 0.1, (b) x = 0.2, (c) x = 0.2, and (d) x = 0.8 ceramics. (e) Crystal structures of M and T phases of AVO_4.

To further explain the change in crystal structure induced by doping Ho^{3+}, Raman spectra of all $Bi_{1-x}Ho_xVO_4$ ceramics were collected at room temperature. Raman peak at 823/cm and the weak shoulder at 717/cm for BHV-0.1 ceramic are ascribed to ν_s(V−O) (the symmetric V−O stretching mode, A_g symmetry) and ν_{as}(V−O) (the anti-symmetric V−O stretching mode, B_g symmetry), respectively [9, 21]. The peaks at 365/cm and 331/cm are ascribed to the $\delta_s(VO_4)^{3-}$ (the symmetric A_g bending mode) and $\delta_{as}(VO_4)^{3-}$ (the anti-symmetric B_g bending mode), respectively. External modes (rotation/translation) are represented by the bands below 300/cm [22, 23]. The intensity of the characteristic peak of the T phase at around 887/cm (A_{1g}, ν_1) increases as the Ho^{3+} concentration increases. In general, two sets of Raman spectra were detected in BHV-0.1, 0.15, and 0.2. For BHV-0.9 ceramic, the peak at 811/cm is assigned to the B_{2g} (ν_3), and the 377/cm and 483/cm peaks are assigned to the A_{1g} (ν_2)

and B_{2g} (v_4), respectively. The results of the Raman analysis agree well with those of the XRD analysis.

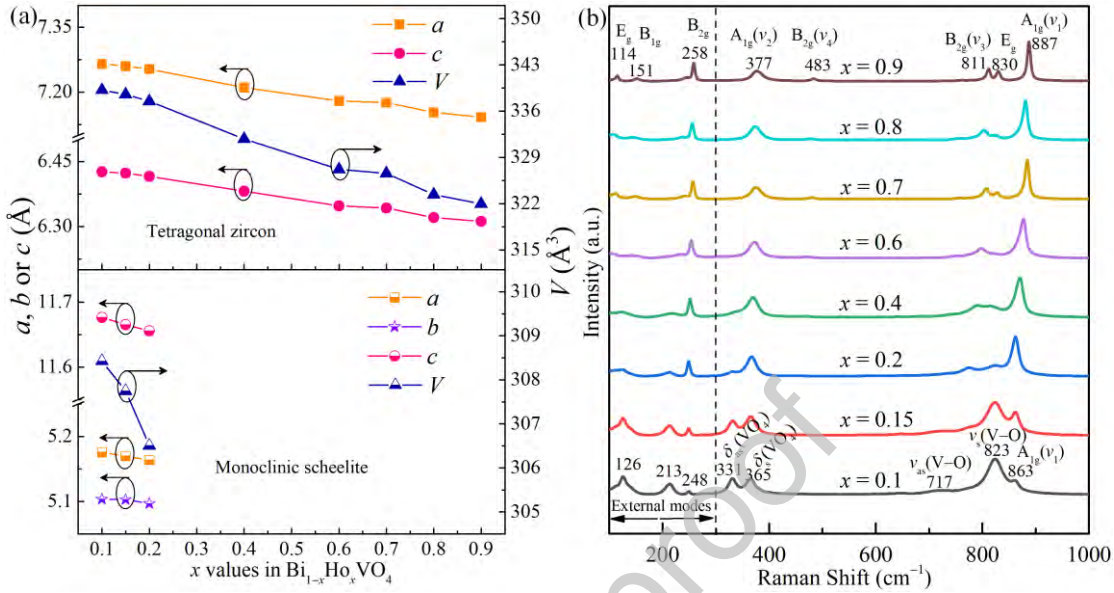

Fig. 3. (a) Lattice parameters (a, b, and c) and unit cell volume (V) of tetragonal phase and monoclinic phase in the $Bi_{1-x}Ho_xVO_4$ ($0.1 \leq x \leq 0.9$) system. (b) Raman spectra of all $Bi_{1-x}Ho_xVO_4$ ceramics at room temperature.

Selected area electron diffraction (SAED) and high-resolution transmission electron microscopy (HR-TEM) images were collected to analyze the local structure of $Bi_{1-x}Ho_xVO_4$ ceramics. Due to the main M with a small T phase, the SAED image of x = 0.10 ceramic shows a typical polycrystalline pattern (Fig. 4(a)). From the HR-TEM image (Fig. 4(b)), the lattice spacing is 0.4791 nm which corresponds to the spacing of the (−101) planes in x = 0.10 ceramic. SAED and HR-TEM images of the x = 0.40 ceramic viewed from the [1−11] direction are shown in Fig. 4(c, d). The interplanar spacings of $d_{(112)}$ and $d_{(220)}$ are estimated to be about 0.2626 and 0.2494 nm, which are slightly lower than the 0.2674 (112) and 0.2518 (220) of PDF card (82-1973), which is caused by the difference in the radii of Bi^{3+} and Ho^{3+}.

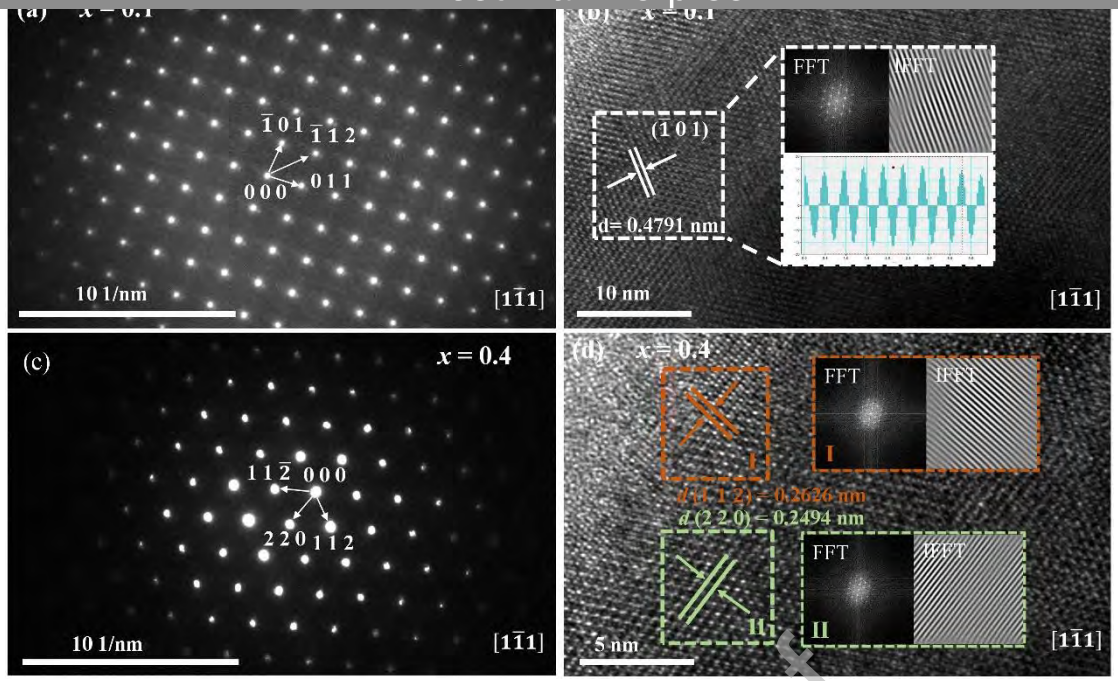

Fig. 4. SAED and HR-TEM images of (a, b) x = 0.1 and (c, d) x = 0.4 viewed from the [1−11] direction. The inset images are the fast Fourier transform map (FFT), inverse fast Fourier transform map (IFFT), and lattice spacing.

The SEM images of the thermally etched surface of the $Bi_{1-x}Ho_xVO_4$ ceramics sintered at optimal temperatures are shown in Fig. 5(a−f). Dense morphology can be observed in all ceramics with few pores, which indicates that the ceramics have a high density at the optimal temperature. Two morphologies of grains are observed in the x = 0.1 and 0.2 samples, with the small columnar grains being T phase and the large sheetar grains being M phase. As x increases, the M phase gradually decreases, and by x = 0.4, the $Bi_{1-x}Ho_xVO_4$ ceramic is fully shown as the T phase, which is consistent with the results of XRD. The calculated average grain size is 0.54 μm at x = 0.4 and then slightly decreases to 0.36 μm at x = 0.9. With the increase of x, the bulk density (6.43−5.64 g/cm^3) and theoretical density (98.09%−96.20%) of $Bi_{1-x}Ho_xVO_4$ ($0.1 \leq x$

≤ 0.9) ceramics gradually decrease (Fig. S2), since the density of $BiVO_4$ of scheelite (6.96 g/cm^3) is greater than that of zircon $HoVO_4$ (5.73 g/cm^3). The relative density of $Bi_{1-x}Ho_xVO_4$ ceramics reaches more than 95%, indicating that the compactness is excellent and consistent with the SEM images.

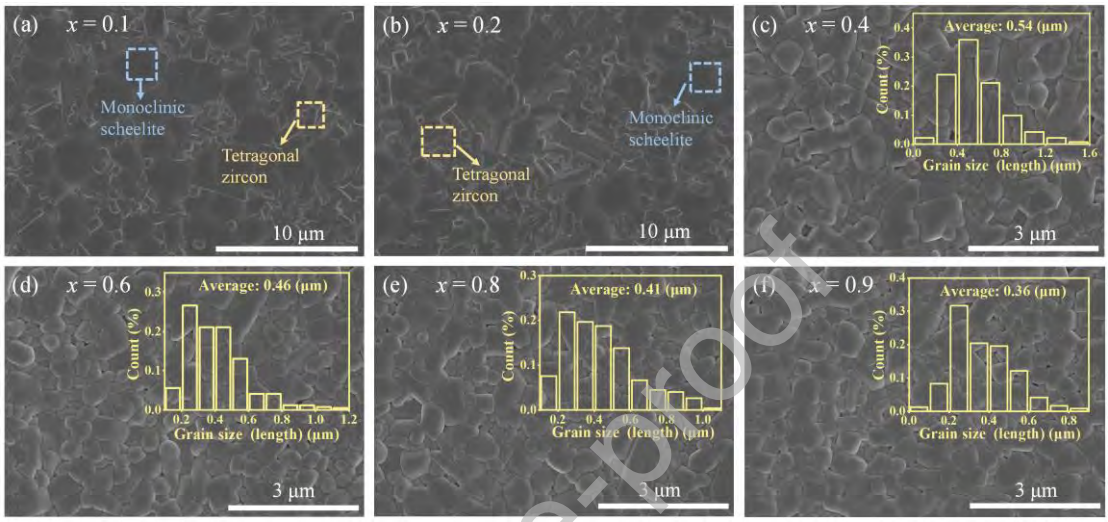

Fig. 5. Surface SEM images of thermally etched $Bi_{1-x}Ho_xVO_4$ ceramics after polishing and the corresponding grain size distributions: (a) x = 0.1, (b) x = 0.2, (c) x = 0.4, (d) x = 0.6, (e) 0.8, and (f) x = 0.9.

As shown in Fig. 6(a), the measured ε_r of $Bi_{1-x}Ho_xVO_4$ ceramics decreases from 58.9 (x = 0.1) to 14.7 (x = 0.9) with the increase of x, mainly because the ε_r depends on the logarithmic rule and molecular polarizability [24−27].

$$\lg\varepsilon_r = V_1 \lg\varepsilon_{r1} + V_2 \lg\varepsilon_{r2} \quad (4)$$

$$\varepsilon_r = \frac{3V_m + 8\pi\alpha_m}{3V_m - 4\pi\alpha_m} \quad (5)$$

$$\alpha_m = (1-x)\alpha(Bi^{3+}) + x\alpha(Ho^{3+}) + \alpha(V^{5+}) + 4\alpha(O^{2-}) \quad (6)$$

where V_1 and V_2 are the volume fractions of monoclinic and tetragonal phases, the ionic polarizabilities are 6.12 Å^3 for Bi^{3+}, 3.97 Å^3 for Ho^{3+}, 2.92 Å^3 for V^{5+}, and 2.01

Å^3 for O^{2-}. The calculated dielectric constant ($\varepsilon_{r(C-M)}$ = 34.3−12.1) shows the same trend as the measured value, both decreasing as x increases and the calculated $\varepsilon_{r(C-M)}$ values being lower than measured ε_r values. As the x value increases, $Q \times f$ increases linearly from 6,500 GHz (x = 0) to 9,400 GHz (x = 0.15, f = 5.81 GHz), then decreases to 6,400 GHz (x = 0.2, f = 6.41 GHz) and increases again to 21,900 GHz (f = 9.59 GHz) at x = 0.7, then decreases to 9,200 GHz (f = 11.06 GHz) at x = 0.9, finally increases again (Fig. 6(b)). The $Q \times f$ value is usually affected by many aspects, such as the second phase, defects, and phonon oscillation in the lattice [28−30], and compared with the situation in the solid solution, the $Q \times f$ in the composite material is usually unable to obtain simple linear results.

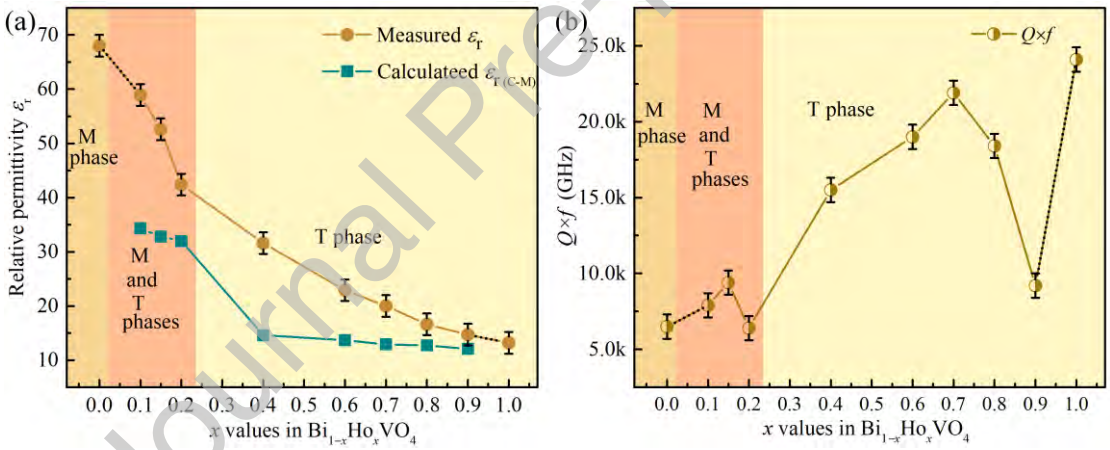

Fig. 6. Variation in (a) relative permittivity and (b) $Q \times f$ of $Bi_{1-x}Ho_xVO_4$ ceramics at their optimum temperature as a function of x value.

To investigate the intrinsic microwave dielectric properties, the infrared reflectivity spectra of $Bi_{1-x}Ho_xVO_4$ (x = 0.2 and 0.7) ceramics were analyzed using a classical harmonic oscillator model [31]:

$$\varepsilon^*(\omega) = \varepsilon_\infty + \sum_{j=1}^{n} \frac{\omega_{pj}^2}{\omega_{oj}^2 - \omega^2 - j\gamma_j\omega} \quad (7)$$

where $\varepsilon^*(\omega)$ is the complex dielectric function, ε_∞ is the dielectric constant caused by

the electronic polarization at high frequencies, γ_j, ω_{oj}, and ω_{pj} are the damping factor, the transverse frequency, and plasma frequency of the j-th Lorentz oscillator, respectively. The complex reflectivity $R(\omega)$ can be written as [32]:

$$R(\omega) = \left| \frac{1-\sqrt{\varepsilon^*(\omega)}}{1+\sqrt{\varepsilon^*(\omega)}} \right|^2 \quad (8)$$

In the microwave frequency region ($\omega << \omega_{oj}$), the real and imaginary parts of the complex permittivity and dielectric loss ($\tan\delta$) can be written as follows [33]:

$$\varepsilon'(\omega) = \varepsilon_\infty + \sum_{j=1}^{n} \varepsilon_j = \varepsilon_\infty + \sum_{j=1}^{n} \frac{\omega_{pj}^2}{\omega_{oj}^2} \quad (9)$$

$$\varepsilon''(\omega) = \sum_{j=1}^{n} \frac{\omega_{pj}^2 \omega \gamma_j}{\omega_{oj}^2} \quad (10)$$

$$\tan\delta = \frac{\varepsilon''}{\varepsilon'} = \omega \sum_{j=1}^{n} \frac{\Delta\varepsilon_j \gamma_j}{\omega_{oj}^2 (\varepsilon_\infty + \sum_{j=1}^{n} \Delta\varepsilon_j)} \quad (11)$$

Fig. 7 shows the fitted infrared reflectivity values and the complex permittivities of $Bi_{1-x}Ho_xVO_4$, and the relevant parameters are listed in Table S2. The fitted ε' values (48.8 and 22.8) of BHV-0.2 and BHV-0.7 ceramics are closer to the measured ε_r values (42.4 and 20.0) compared to the calculated $\varepsilon_{r(C-M)}$ values (32.0 and 12.9). The calculated $\tan\delta$ values of BHV-0.2 and BHV-0.7 ceramics are 6.84×10^{-4} (at 5.82 GHz) and 1.16×10^{-3} (at 11.34 GHz), which are almost equal to the measured ones using TE_{011} method, indicating that the majority of the dielectric contribution for $Bi_{1-x}Ho_xVO_4$ at microwave region was attributed to the absorption of phonon oscillation at the infrared region.

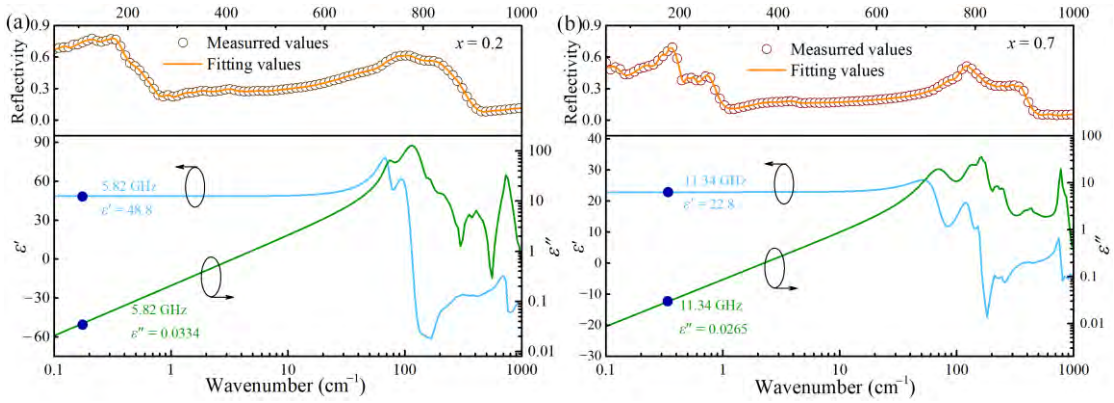

Fig. 7. Measured and calculated infrared reflectivity spectra and fitted complex dielectric spectra of (a) BHV-0.2 and (b) BHV-0.7 ceramics.

Generally, the relative permittivity of ceramics strongly depends on the distance between cations and anions, which can be evaluated effectively by the bond valence because the bond valence is a function of bond length and bond strength between cation and anion [34]. Bond valences (V_i) are calculated using bond distance (d_{ij}), bond valence parameter (R_{ij}), and the constant b, as follows [35,36]:

$$V_i = \sum_j v_{ij} \quad (12)$$

$$v_{ij} = \exp\left[\frac{R_{ij} - d_{ij}}{b}\right] \quad (13)$$

The bond valence of each cation in $Bi_{1-x}Ho_xVO_4$ ceramics is listed in Table 1 and Table S3. In the M structure, the bond valence of Ho^{3+} (2.3558−2.2038 v.u.) and Bi^{3+} (2.8234−2.6413 v.u.) is less than the theoretical value (+3 v.u.), which suggests that they are both small in the [AO_8] dodecahedron, i.e., to show a tendency to be rattling cations. However, V^{5+} shows the bond valence of 5.5771−6.4894 v.u., suggesting it is tightly bound in the [VO_4] tetrahedral site (compressed). In the T structure, Ho^{3+} (2.8178−2.8806 v.u.) is in a rattling state, Bi^{3+} (3.3771−3.4524 v.u.) is compressed, and V^{5+} (4.6700−5.8681 v.u.) gradually changes from rattling to compression.

Therefore, the main reason for $\varepsilon_r > \varepsilon_{r(C-M)}$ is the rattling of Ho^{3+} in the dodecahedron, and the narrowing of the deviation between them as x increases might be related to the gradual compression of V^{5+} in the tetrahedron.

Table 1. Bond valence of each cation in $Bi_{1-x}Ho_xVO_4$ ceramics.

	Monoclinic structure			Tetragonal structure		
x values	V_{Ho}^{3+} (v.u.)	V_{Bi}^{3+} (v.u.)	V_V^{5+} (v.u.)	V_{Ho}^{3+} (v.u.)	V_{Bi}^{3+} (v.u.)	V_V^{5+} (v.u.)
0.1	2.3558	2.8234	5.5771	2.8178	3.3771	4.6700
0.15	2.3691	2.8394	5.5668	2.9106	3.4885	4.4266
0.2	2.2038	2.6413	6.4894	2.5655	3.0748	5.5473
0.4	/	/	/	2.5567	3.0642	6.1473
0.6	/	/	/	2.7246	3.2654	5.9431
0.7	/	/	/	2.8812	3.4531	5.4832
0.8	/	/	/	2.9266	3.5075	5.6106
0.9	/	/	/	2.8806	3.4524	5.8681

As shown in Fig. 8(a), the τ_f of $Bi_{1-x}Ho_xVO_4$ first increases from a negative value (−140.4 ppm/°C at x = 0.1) to a positive value (+76.68 ppm/°C at x = 0.4) and then decreases from a positive value to a negative value (−6.40 ppm/°C at x = 0.9). Therefore, two points with zero τ_f appear in $Bi_{1-x}Ho_xVO_4$ ($0 \le x \le 1$) ceramics, about x = 0.17 and 0.83, respectively. Obviously, the τ_f change of $Bi_{1-x}Ho_xVO_4$ ceramics does not conform to the two-phase composite law and the average ion polarizability dilution theory (τ_f = −260 ppm/°C for $BiVO_4$ and τ_f = −17.4 ppm/°C for $HoVO_4$). The

τ_f is a function of both τ_ε and the linear thermal expansion coefficient (α_L), as follows [37, 38]:

$$\tau_f = -\left(\alpha_L + \frac{1}{2}\tau_\varepsilon\right) \quad (14)$$

$$\tau_\varepsilon = \frac{1}{\varepsilon_r}\left(\frac{\partial \varepsilon_r}{\partial T}\right) = \frac{(\varepsilon_r - 1)(\varepsilon_r + 2)}{3\varepsilon_r}\left(\frac{1}{\alpha_m}\frac{d\alpha_m[T,V(T)]}{dT} - 3\alpha_L\right) \quad (15)$$

$$\frac{1}{\alpha_m}\frac{d\alpha_m[T,V(T)]}{dT} = \frac{1}{\alpha_m}\left(\frac{\partial \alpha_m}{\partial T}\right)_V + \frac{1}{\alpha_m}\left(\frac{\partial \alpha_m}{\partial V}\right)_T\left(\frac{\partial V}{\partial T}\right)_P = A + B = \tau_{\alpha m} \quad (16)$$

where A represents the direct dependence of the polarizability on temperature, and B represents the relationship between polarizability and volume expansion. In fact, ionic polarizability varies with simultaneous changes in volume and temperature. Therefore, we combined $A+B$ (i.e., temperature coefficient of ionic polarizability $\tau_{\alpha m}$) to study the influence mechanism of τ_ε and τ_f. As shown in Fig. 8(b) and Table 2, the α_L values of $Bi_{1-x}Ho_xVO_4$ increase from 9.2 to 10.9 ppm/°C and then decrease to 7.7 ppm/°C between 25 and 500 °C. The $\tau_{\alpha m}$ values decrease from 40.75 ppm/°C (x = 0.1) to 16.55 ppm/°C (x = 0.4) and then increase to 21.03 ppm/°C (x = 0.4) (Table 2). When x = 0−0.4, the rattling effects of Ho^{3+} and Bi^{3+} cations are increased, and the influence of temperature on ion polarization is gradually enhanced. When x > 0.4, the rattling effects of Ho^{3+} and Bi^{3+} cations are weakened, and the influence of volume on ion polarization is gradually enhanced. Therefore, the change in $\tau_{\alpha m}$ caused by the rattling effect of cations is the physical nature that affects τ_f.

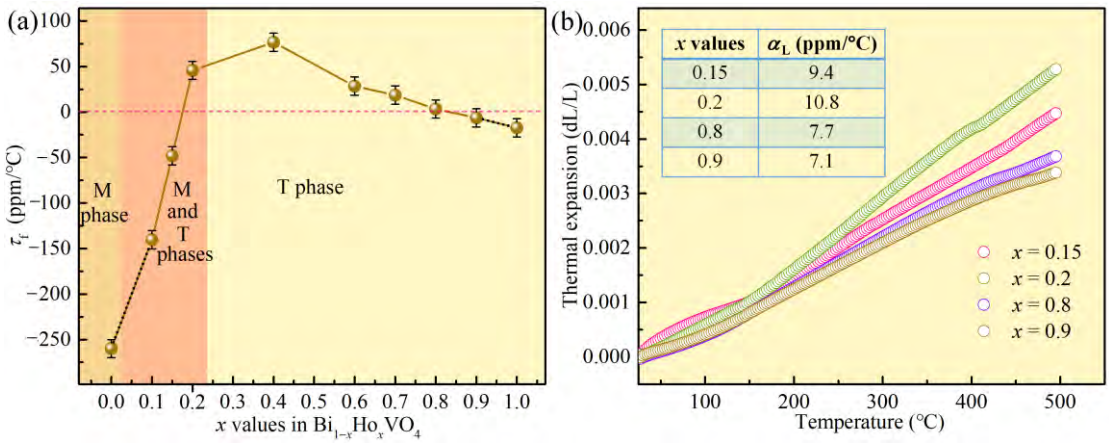

Fig. 8. (a) The τ_f of $Bi_{1-x}Ho_xVO_4$ ceramics as a function of x value. (b) Thermal expansion data of the $Bi_{1-x}Ho_xVO_4$ ceramics.

Table 2. τ_ε, α_L, $\tau_{\alpha m}$-3α_L, and τ_f values of $Bi_{1-x}Ho_xVO_4$ ceramics (ppm/°C).

x values	α_L	τ_ε	$\tau_{\alpha m}$	$\tau_{\alpha m}$-3α_L	τ_f
0.1	9.20	262.40	40.75	13.15	−140.40
0.15	9.40	77.36	32.53	4.33	−48.08
0.2	10.80	−113.16	24.57	−7.83	+45.78
0.4	10.90	−175.16	16.55	−16.15	+76.68
0.6	8.70	−74.34	16.73	−9.37	+28.47
0.7	8.30	−53.82	17.17	−7.73	+18.61
0.8	7.70	−21.98	19.33	−3.77	+3.29
0.9	7.10	−1.40	21.03	−0.27	−6.40

As we all know, M $BiVO_4$ has been widely researched for applications in antennas, filters, and resonators due to its low melting temperature (820 °C) and promising microwave dielectric properties (ε_r = 68, $Q \times f$ = 6,800 GHz and τ_f = −260 ppm/°C) [8,39]. Unfortunately, $BiVO_4$ reacts with Ag electrode at the sintering temperature and

has a large negative τ_f, both of which preclude its use in LTCC technology [40]. Because $Bi_{0.3}Ho_{0.7}VO_4$ has a sintering temperature slightly lower than the melting point of the Ag (961 °C) electrode, it has the potential to be used in LTCC technology. Cofiring with Ag (in 20 wt.%) was done by sintering at 960 °C to test the chemical compatibility of $Bi_{0.3}Ho_{0.7}VO_4$ with Ag electrode. The XRD pattern only shows diffraction peaks of $Bi_{0.3}Ho_{0.7}VO_4$ and Ag, confirming that no chemical reaction occurs between them, as shown in Fig. 9(a). Only two grains of different morphologies are observed in the backscattered electron (BSE) image, which belongs to the $Bi_{0.3}Ho_{0.7}VO_4$ and Ag, respectively (Fig. 9(b)). 80 wt.%$Bi_{0.3}Ho_{0.7}VO_4$-20 wt.%Ag composition sintered at 960 °C exhibit good microwave dielectric properties with ε_r = 17.9, $Q \times f$ = 13,500 GHz, and τ_f = + 21.7 ppm/°C. These results indicate that Ho^{3+} can improve the chemical compatibility of $Bi_{1-x}Ho_xVO_4$ and Ag, and $Bi_{0.3}Ho_{0.7}VO_4$ is a promising LTCC material.

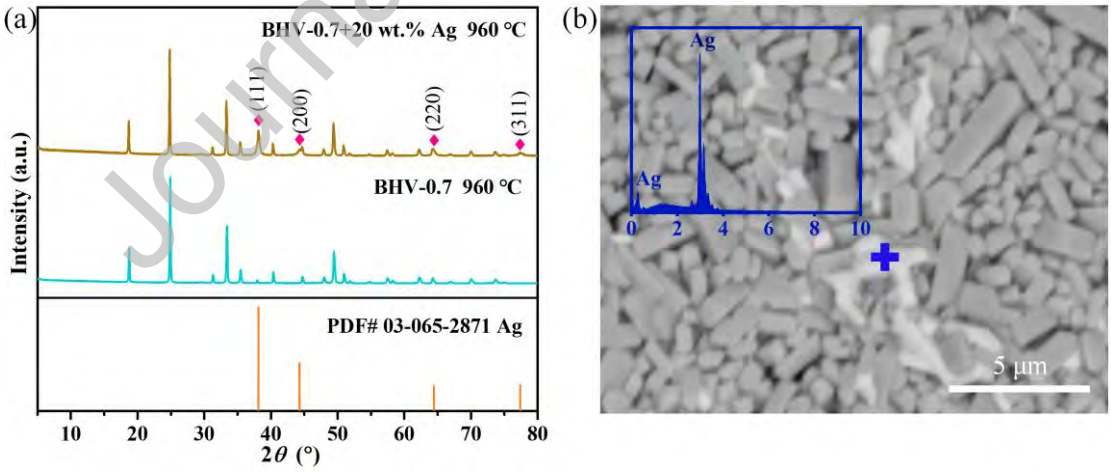

Fig. 9. (a) XRD patterns of the cofired $Bi_{0.3}Ho_{0.7}VO_4$ with Ag. (b) BSE image and EDS analysis of 80 wt.%$Bi_{0.3}Ho_{0.7}VO_4$-20 wt.%Ag.

4. Conclusions

The $Bi_{1-x}Ho_xVO_4$ ceramics comprised M and T phases in the range of $0.1 \leq x < 0.4$, and a T phase could be obtained when $x \geq 0.4$. The measured ε_r and calculated $\varepsilon_{r(C-M)}$ of $Bi_{1-x}Ho_xVO_4$ ceramics decrease from 58.9 and 34.1 ($x = 0.1$) to 14.7 and 12.1 ($x = 0.9$), which depends on the logarithmic rule and molecular polarizability. Bond valence analysis shows that the main reason for $\varepsilon_r > \varepsilon_{r(C-M)}$ is the rattling of Ho^{3+} in the dodecahedron, and the narrowing of the deviation between them as x increases might be related to the gradual compression of V^{5+} in the tetrahedron. The $Q \times f$ does not change linearly with the x increase and is mainly affected by the absorption of phonon oscillation in the infrared region, complex phase, and cation rattling. The τ_f increased from a negative (−140.4 ppm/°C at $x = 0.1$) to a positive (+76.68 ppm/°C at $x = 0.4$) and then decreased to a negative value (−6.40 ppm/°C at $x = 0.9$). Therefore, two points with zero τ_f appeared in $Bi_{1-x}Ho_xVO_4$ ($0 \leq x \leq 1$) ceramics, about $x = 0.17$ and 0.83, respectively. The best microwave dielectric properties with $\varepsilon_r = 16.6$, $Q \times f =$ 18,400 GHz (f = 10.69 GHz), and τ_f = +3.29 ppm/°C were obtained in the $Bi_{0.2}Ho_{0.8}VO_4$ ceramic. The change in $\tau_{\alpha m}$ caused by the rattling effect of cations is the physical essence that affects τ_f. Therefore, the rattling effect can be used as an effective mechanism to regulate τ_f in low-ε_r materials. By XRD, BES, and EDS analyses, it is confirmed that no chemical reaction occurs between $Bi_{1-x}Ho_xVO_4$ and Ag electrode, which indicates that $Bi_{1-x}Ho_xVO_4$ can be used as a potential dielectric resonance material in microwave communication and LTCC technology.

Acknowledgments

This work was supported by the Natural Science Foundation of Guangxi Zhuang

Autonomous Region (No. 2023GXNSFBA026076), the Guangxi Key Laboratory of Optical and Electronic Materials and Devices (No. 22KF-10), the Natural Science Foundation of China (Nos. 21965009 and 22105048), the Guilin University of Technology Research Startup Project (No. GUTQDJJ2021073), and the Guangxi BaGui Scholars Special Funding.

References

[1] H. Xiang, J. Kilpijärvi, S. Myllymäki, H. Yang, L. Fang, H. Jantunen, Appl. Mater. Today 21 (2020) 100826.

[2] F.F. Wu, D. Zhou, C. Du, D.M. Xu, R.T. Li, Z.Q. Shi, M.A. Darwish, T. Zhou, H. Jantunen, Chem. Mater. 35 (2023) 104−115.

[3] C. Yin, Y. Yin, K. Du, X. Song, H. Guo, Y. Xiong, M. Cheng, J. Yang, W. Luo, W. Lu, W. Lei, C. Li, J. Eur. Ceram. Soc. 43 (2023) 1492−1499.

[4] Y. Sadin, E. Taheri-Nassaj, R. Schmidt, A. Yourdkhani, S. Myllymäki, H. Jantunen, H. Barzegar-Barfrooei, J. Eur. Ceram. Soc. 44 (2024) 1617−1626.

[5] H. Xiang, L. Yao, J. Chen, A. Yang, H. Yang, L. Fang, J. Mater. Sci. Technol. 98 (2021) 28−32.

[6] A.K. Bhattacharya, K.K. Mallick, A. Hartridge, Mater. Lett. 30 (1997) 7−13.

[7] M. Valant, D. Suvorov, J. Am. Ceram. Soc. 83 (2000) 2721−2729.

[8] S.H. Wee, D.W. Kim, S.I. Yoo, J. Am. Ceram. Soc. 87 (2014) 871−874.

[9] D. Zhou, W.B. Li, H.H. Xi, L.X. Pang, G.S. Pang, J. Mater. Chem. C 3 (2015) 2582.

[10] D. Zhou, L.X. Pang, J. Guo, Z.M. Qi, T. Shao, Q.P. Wang, H.D. Xie, X. Yao, C.A. Randall, Inorg. Chem. 53 (2014) 1048−1055.

[11] H.H. Guo, D. Zhou, W.F, Liu, L.X. Pang, D.W. Wang, J.Z. Su, Z.M. Qi, J. Am. Ceram. Soc. 103 (2020) 423−431.

[12] E.L. Colla, I.M. Reaney, N. Setter, J. Appl. Phys. 74 (1993) 3414−3425.

[13] A.J. Bosman, E.E. Havinga, Phys. Rev. 129 (1963) 1593.

[14] P.J. Harrop, J. Mater. Sci. 4 (1969) 370−374.

[15] P.L. Wise, I. M. Reaney, W.E. Lee, D.M. Iddles, D.S. Cannell, T.J. Price, J. Mater. Res. 17 (2002) 2033−2040.

[16] Y. Tang, Z.W. Zhang, J. Li, M.Y. Xu, Y.F. Zhai, L. Duan, C.X. Su, L.J. Liu, Y.H. Sun, L. Fang, J. Eur. Ceram. Soc. 40 (2020) 3989−3995.

[17] Y. Jiang, G. Wu, M. Mao, R. Muhammad, W. Sheng, B. Liu, H.B. Bafrooei, E. Taheri-Nassaj, K. Song, Ceram. Int. 49 (2023) 23334−23339.

[18] L. Ao, Y. Tang, J. Li, W. Fang, L. Duan, C. Su, Y. Sun, L. Fang, J. Eur. Ceram. Soc. 40 (2020) 5498−5503.

[19] D. Zhou, L.X. Pang, D.W. Wanga, I.M. Reaney, J. Mater. Chem. C 3 (2015) 2582−2588.

[20] D. Zhou, H. Wang, X. Yao, X. Wei, F. Xiang, L. Pang, Appl. Phys. Lett. 90 (2007) 172910.

[21] R.L. Frost, D.A. Henry, M.L. Weier, W. Martens, J. Raman Spectrosc. 37 (2006) 722−732.

[22] A. Zhang, J. Zhang, N. Cui, X. Tie, Y. An, L. Li, J. Mol. Catal. A-Chem. 304 (2009) 28−32.

[23] J. Yu, A. Kudo, Adv. Funct. Mater. 16 (2006) 2163−2169.

[24] S.V. Trukhanov, I.O. Troyanchuk, N.V. Pushkarev, H. Szymczak, J. Exp. Theor. Phys. 95 (2002) 308−315.

[25] S.H. Yoon, G.K. Choi, D.W. Kim, S.Y. Cho, K.S. Hong, J. Eur. Ceram. Soc. 27 (2007) 3087−3091.

[26] P.V. Rysselberghe, J. Phys. Chem. 36 (1932) 1152−1155.

[27] R.D. Shannon, J. Appl. Phys. 73 (1993) 348−366.

[28] W. Wang, M. Shehbaz, X. Wang, C. Du, D. Xu, Z.Q. Shi, M.A. Darwish, H.S. Qiu, B.B. Jin, T. Zhou, Y.W. Chen, Q.X. Liang, M.R. Zhang, D. Zhou, ACS Appl. Mater. Interfaces 15 (2023) 51453−51461.

[29] K. Du, C. Yin, Z. Zou, M. Cheng, Y. Cai, J. Yang, M. Zhang, W. Lu, S. Wang, W. Lei, J. Am. Ceram. Soc. 106 (2023) 5822−5831.

[30] J. Bao, Y. Zhang, H. Kimura, H. Wu, Z. Yue, J. Adv. Ceram. 12 (2023) 82−92.

[31] K. Wakino, M. Murata, H. Tamura, J. Am. Ceram. Soc. 69 (1986) 34−37.

[32] S. Kamba, H. Wang, M. Berta, F. Kadlec, J. Petzelt, D. Zhou, X. Yao, J. Eur. Ceram. Soc. 26 (2006) 2861−2865.

[33] Y.D. Dai, G.H. Zha, H.X. Liu, J. Appl. Phys. 105 (2009) 034111.

[34] E.S. Kim, S.H. Kim, J. Electroceram. 21 (2008) 2−7.

[35] I.D. Brown, Chem. Soc. Rev. 7 (1978) 359−376.

[36] N.E. Brese, M. O'keeffe, Acta Crystallogr. 47 (1991) 192−197.

[37] A.J. Bosman, E.E. Havinga, Phys. Rev. 129 (1963) 1593−1600.

[38] H. Xiang, C. Li, H. Jantunen, L. Fang, A.E. Hill, ACS Sustain. Chem. Eng. 6 (2018) 6458−6466.

[39] F.F. Wu, D. Zhou, S. Xia, L. Zhang, F. Qiao, L.X. Pang, S.K. Sun, T. Zhou, C. Singh, A.S.B. Sombra, M.A. Darwish, I.M. Reaney, J. Eur. Ceram. Soc. 42 (2022) 5731−5737.

[40] M.T. Sebastian, H. Jantunen, Int. Mater. Rev. 53 (2013) 57−90.

Graphical abstract

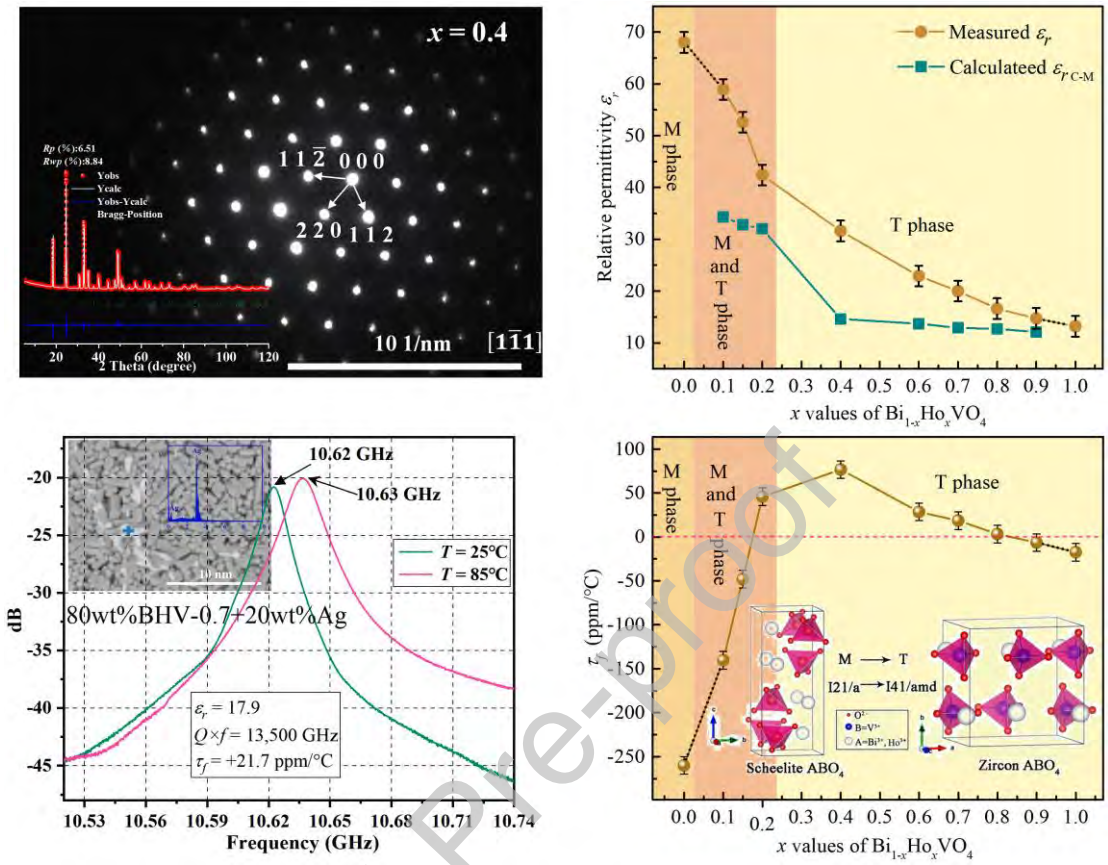

Declaration of interests

☒ The authors declare that they have no known competing financial interests or personal relationships that could have appeared to influence the work reported in this paper.

☐ The author is an Editorial Board Member/Editor-in-Chief/Associate Editor/Guest Editor for [Journal name] and was not involved in the editorial review or the decision to publish this article.

☐ The authors declare the following financial interests/personal relationships which may be considered as potential competing interests: